Dispersive spectrum and orbital order of spinless *p*-band fermions in an optical lattice

Xiancong Lu and E. Arrigoni

Institute of Theoretical and Computational Physics, Graz University of Technology, A-8010 Graz, Austria

We study single-particle properties of a spinless *p*-band correlated fermionic gas in an optical lattice by means of a variational cluster approach (VCA). The single-particle spectral function is almost flat at half filling and develops a strongly dispersive behavior at lower fillings. The competition between different orbital orderings is studied as a function of filling. We observe that an "antiferromagnetic" orbital order develops at half filling and is destroyed by doping the system evolving into a disordered orbital state. At low-filling limit, we discuss the possibility of "ferromagnetic" orbital order by complementing the VCA result with observations based on a trial wave function. We also study the behavior of the momentum distribution for different values of the on-site interaction. Finally, we introduce an integration contour in the complex plane which allows to efficiently carry out Matsubara frequency sums.

I. INTRODUCTION

Ultracold atomic gases in optical lattices constitute a promising system to simulate and investigate strongly correlated quantum phases as a function of their model parameters, which can be controlled experimentally in a large range.[1] This field of research has greatly expanded after the pioneering realization of the Superfluid to Mott insulator transition by loading bosonic atoms to the lowest band of optical lattices.[2,3] Recent progress in this field has been achieved by loading the atoms in the first-excited band, which makes the study of orbital physics possible in these systems.[4–6] Orbital degrees of freedom play an important role in many solid-state materials: many interesting phenomena such as metal-insulator transitions,[7] superconductivity,[8] colossal magnetoresistance,[9] and half metallicity,[10,11] are rooted in the coupling of orbital with the other degrees of freedom (spin, charge, and phonon). The study of orbital physics in optical lattices, in a pure and tunable environment, is believed to be of great help to understand the complicated orbital issue of solid-state systems.

The basic physics of cold atoms in the first-excited band can be captured by a *p*-band Hubbard-like Hamiltonian.[5,6] Many novel phenomena and quantum phases have been predicted for the *p*-band bosons,[5,6,12–15] e.g., quantum stripe order,[12] Wigner crystallization,[14] and bond algebraic liquid phase.[15] For the spin 1/2 *p*-band fermions, an antiferromagnetic order was found at half filling in both the strong and weak-interaction regimes,[16] and a robust ferromagnetic order was shown to exist for a large range of interaction and at band filling lower than half filling.[17] Itinerant ferromagnetism was also proposed in the honeycomb lattices in Ref. 18. Experimentally, the population of higher band was studied by Browaeys *et al.*[19] and Köhl *et al.*[20] for bosons and fermions, respectively. Recent experiments performed by Müller *et al.*[4] were able to realize long lifetime *p*-band orbital bosonic systems.

In particular, the orbital exchange physics in the Mott state of an orbital-only model, which is realized by loading the single-component (spinless) fermions into *p*-band optical lattices [see the Hamiltonian in Eq. (1)], has been studied by

Zhao *et al.*[21] and Wu[22] for various geometry lattices. In these works, a new orbital exchange mechanism was found, and long-range orbital order was predicted. At the same time, a similar orbital-only model was proposed to describe the ferromagnetic plane in transition-metal oxides with t_{2g} orbital degeneracy, such as Sr_2VO_4 and K_2CuF_4.[23] The spectral properties of this model in the half-filled case have been studied, and it was shown that a hole in a background of antiferromagnetic orbital order does not localize but moves coherently due to an effective three-site hopping term.

Motivated by these previous works, we study numerically this spinless *p*-band model on a square lattice with an emphasis on the excitation spectrum and orbital order away from half filling. The paper is organized as follows: In Sec. II, we present the Hamiltonian of the model, and we briefly summarize the method used to approximately solve it, namely, the variational cluster approach. As a by-product, in this work, we introduce and adopt a more efficient method to carry out sums over Matsubara frequencies, which could also be applied to other problems. Details are given in the Appendix. In Sec. III, we present the calculated results including the single-particle spectrum, orbital orders, and momentum distribution. Finally, we draw our conclusions in Sec. IV.

II. HAMILTONIAN AND METHOD

We consider an anisotropic three-dimensional (3D) optical lattice with optical trapping frequency $\omega_z \gg \omega_x = \omega_y$, so that the dynamics in the *z* direction is essentially suppressed. Supposing that the lowest *s* orbital of the optical lattice is fully occupied by fermions, the other particles can only fill the degenerate p_x and p_y orbitals.[21,22] A fermionic gas, which is polarized into a single hyperfine spin state by magnetic field and loaded in such optical lattice, can be described by the following two-dimensional (2D) spinless *p*-band Hubbard Hamiltonian:

$$H = \sum_{\mathbf{r}} \sum_{\alpha,\beta=x,y} t_{\alpha\beta}(c^{\dagger}_{\mathbf{r},\alpha}c_{\mathbf{r}+\hat{\mathbf{e}}_{\beta},\alpha} + \text{H.c.}) + U\sum_{\mathbf{r}} n_{\mathbf{r},x}n_{\mathbf{r},y}. \quad (1)$$

Here, $c^{\dagger}_{\mathbf{r},\alpha}$ creates a fermionic atom in the p_{α} orbital at position $\mathbf{r}$, $\hat{\mathbf{e}}_{\beta}$ is the unit vector of the β direction (the lattice
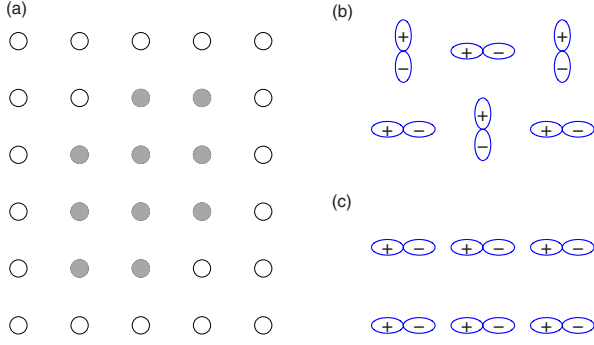
FIG. 1. (Color online) Reference cluster for the VCA calculation (a) consisting of $L=10$ sites (gray). Schematic representation of "antiferromagnetic" (b), and of "ferromagnetic" orbital orders (c).

spacing is set equal to unity), $t_{\alpha\beta}=t_{\parallel}\delta_{\alpha\beta}+t_{\perp}(1-\delta_{\alpha\beta})$ is the hopping amplitude of orbital p_α in direction β, and U is the on-site repulsive interaction between atoms in different orbitals. The longitudinal hopping $t_{\parallel}$ is positive but the transverse hopping $t_{\perp}$ is negative because of the odd parity of p orbitals.[21,22] In general, one has $|t_{\parallel}| \gg |t_{\perp}|$ for the strongly anisotropic shape of p orbital, therefore, we choose a typical small value $t_{\perp}=-0.05t_{\parallel}$ in our calculation[14,16] and set $t_{\parallel}$ as the energy scale. Obviously, in the limit $t_{\perp} \to 0$ the hopping will be restricted to one dimension and the number of particles in a given orbital (p_α) will be conserved for each chain oriented along α. There is no s-wave scattering for atoms in a single hyperfine spin state because of the Pauli exclusion principle. Therefore, the interaction U between atoms mainly comes from p-wave scattering, whose strength can be tuned using a p-wave Feshbach resonance.[21] It is argued that U can be increased to the order of the recoil energy E_R in the present experiment.[24]

The variational cluster approach (VCA) (Refs. 25 and 26) is an extension of cluster perturbation theory (CPT).[27–29] Within CPT, the original lattice is divided into a set of disconnected clusters, and the intercluster hopping parameters are treated perturbatively. Within VCA, additional ("virtual") single-particle terms are added to the cluster Hamiltonian, to obtain a so-called reference system, and then subtracted perturbatively (so that if the perturbative treatment was exact, results would not depend on these terms). These single-particle terms can contain "Weiss" fields to describe a particular ordered state, but also other Hamiltonian parameters, such as an offset in the chemical potential between the cluster and the lattice. The "optimal" value for these variational parameters is determined, in the framework of self-energy functional approach (SFA),[30,31] by requiring that the SFA grand canonical potential

$$\Omega = \Omega' + \mathrm{Tr}\ln(\mathbf{G}_0^{-1} - \mathbf{\Sigma})^{-1} - \mathrm{Tr}\ln\mathbf{G}' \qquad (2)$$

is stationary within this set of variational parameters. Here, $\mathbf{G}_0$ is the noninteracting Green's function, Ω', $\mathbf{\Sigma}$, and $\mathbf{G}'$ are the grand canonical potential, self-energy, and Green's function of the reference system, respectively. In this paper, a $L=10$ sites cluster [Fig. 1(a)] is chosen as a reference system and is solved exactly by Lanczos diagonalization method to obtain the reference self-energy. All our calculations are per-

formed at zero temperature for the difficulty of including the temperature effect into Lanczos method. Since we are looking for orbital ordering, an orbital ferromagnetic or antiferromagnetic field is used as a variational parameter, in addition to the cluster on-site energy. The latter is necessary in order to obtain a thermodynamically consistent particle density.[32,33]

The trace in Eq. (2) implicitly contains a sum over Matsubara frequencies which need to be carried out with high accuracy. In connection with a Lanczos diagonalization of the cluster Hamiltonian this can be done by means of the sum over the single-particle excitation energies obtained by the *band Lanczos*[34] method, as explained in Ref. 35 (see also Ref. 36). Alternatively, the same accuracy can be obtained more efficiently by integration over an appropriate contour of the complex-frequency plane, as discussed in the Appendix. Notice that although the contour (see Fig. 6) mainly runs at a finite distance δ from the real axis in order to avoid sharp structures in the spectral function in the $\delta \to 0$ limit, the procedure is exact. There is no need to carry out a $\delta \to 0$ extrapolation: this is exactly contained in the additional contributions from the "vertical" paths (C_3, C_3', C_5, C_5', and C_7 and C_7' in Fig. 6) (see Appendix for details).

III. RESULTS

A. Filling dependent single-particle spectral function

In order to gain insight on the physical properties of the spinless p-band Hubbard model [Eq. (1)], in this section, we calculate its single-particle spectral function using VCA. The VCA has been shown to be an effective method to evaluate the single-particle[26,37] and two-particle[38] spectral function of Hubbard-like models. The filling-dependent spectral function of the p_x orbital with interaction $U=8t_{\parallel}$ is displayed in Fig. 2. By symmetry reasons, the spectrum of the p_y orbital in the nonferromagnetic phase is obtained by interchanging k_x with k_y. The spectra at different fillings are obtained in the respective stable phase, according to the phase diagram displayed in Fig. 4 (see Sec. III B). The spectrum of the p_x orbital is almost k independent in the k_y direction of the Brillouin zone (BZ), since the dispersion is nearly one dimensional (1D). This is quite obviously due to the fact that the transverse hopping ($t_{\perp}=-0.05t_{\parallel}$) is very small. For all fillings, we can clearly recognize the upper and lower Hubbard bands with a gap on the order of U.

At half filling, the spectrum has a ladder structure [see Fig. 2(a)], which is also characteristic of the $t-J^z$ model.[21,23,39] However, the spectrum is slightly dispersive in the k_x direction of the BZ, that is, a hole or particle is not localized but moves coherently through the lattice. The small dispersion can be explained by including a three-sites term in the $t-J^z$ Hamiltonian.[23] More spectra at half filling and for different interactions are given in Fig. 3. The gap between upper and lower Hubbard bands decreases as the interaction decreases. At the same time, the bandwidth becomes larger because a hole (or particle) is easier to move when the interaction is smaller.

Away from half filling, the quasiparticle spectrum becomes strongly dispersive (see Fig. 2). The shape of the
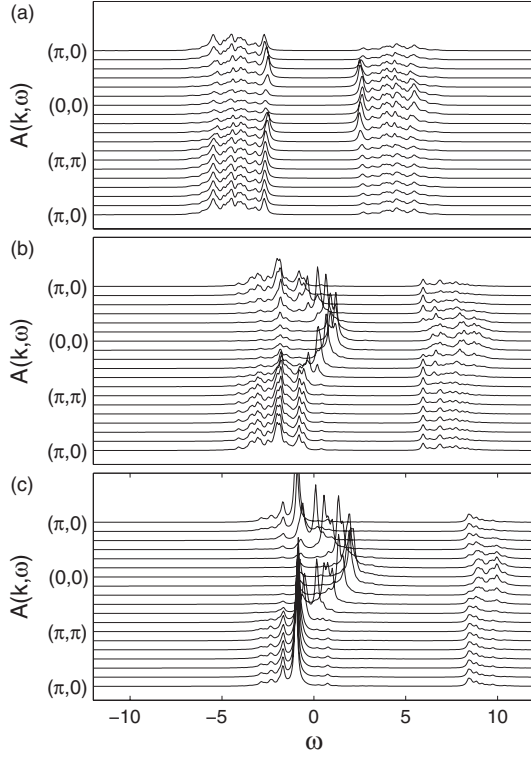
FIG. 2. Single-particle spectral-function $A(\mathbf{k},\omega)$ of p_x orbital at various fillings. From (a)–(c) the fillings of the system are 1.0, 0.8, and 0.6, respectively. The interaction is $U=8t_\parallel$ and the transverse hopping is $t_\perp=-0.05t_\parallel$.

spectrum is similar to that of 1D free particles, but with a strongly renormalized bandwidth. The bandwidth becomes larger and larger when going away from half filling, which means that particles can move easier. Another feature that can be seen in Fig. 2 is the spectral weight-transfer phenomenon between the upper and lower Hubbard bands, which is also observed in the usual single-band Hubbard model.[40] For fillings below half filling [Figs. 2(b) and 2(c)], the spectrum is transferred to the lower Hubbard band. This is because at low density the particles have less chance to doubly occupy the same site and therefore have a smaller probability to be in the upper Hubbard band.[40] Of course, for filling above half filling the situation is reversed due to particle-hole symmetry.

B. Antiferromagnetic orbital order

In this section, we discuss the "antiferromagnetic" orbital order in this model as a function of filling. At half filling and in the strong-coupling limit $U \gg t_\parallel$, the Hamiltonian [Eq. (1)] can be reduced to a superexchange t-J^z model with a positive exchange energy $J=2t_\parallel^2/U$.[21–23] Therefore, the Mott state favors a staggered ("antiferromagnetic") orbital order [see Fig. 1(b)]. To study the orbital order within VCA, we add a "virtual" staggered orbital field, $H'_{AF}=h'_{AF}\Sigma_\mathbf{r}(n_{\mathbf{r},x}-n_{\mathbf{r},y})e^{i\mathbf{Q}\cdot\mathbf{r}}$ with $\mathbf{Q}=(\pi,\pi)$, to the cluster Hamiltonian H'. As explained in Sec. II, this term is then subtracted perturbatively, and the coefficient is determined by optimizing the grand canonical potential [Eq. (2)]. The corresponding staggered orbital order parameter, $m=\Sigma_\mathbf{r}(\langle n_{\mathbf{r},x}\rangle-\langle n_{\mathbf{r},y}\rangle)e^{i\mathbf{Q}\cdot\mathbf{r}}$, is then calculated and
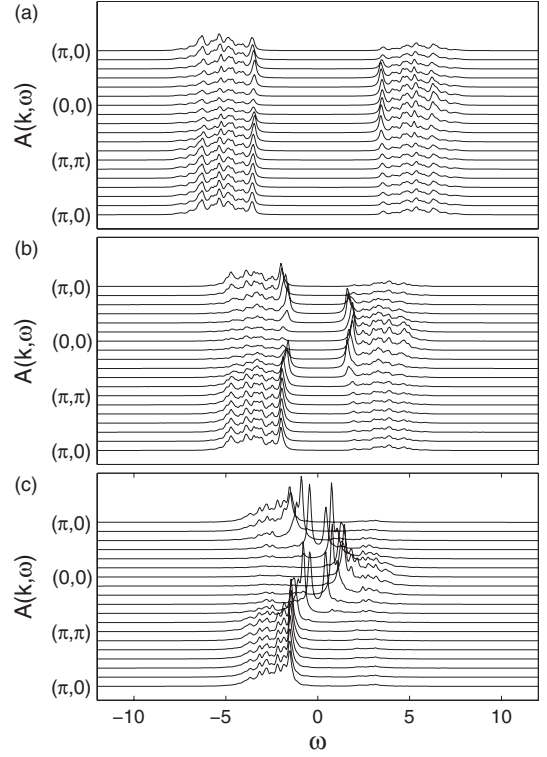

FIG. 3. Single-particle spectral-function $A(\mathbf{k},\omega)$ of the p_x orbital at half filling and for different values of the interaction U. Specifically, we have (a) $U=10t_\parallel$, (b) $6t_\parallel$, and (c) $3t_\parallel$.

plotted in Fig. 4(a) as a function of the interaction U. One can see that the order-parameter m, which is nonzero for any finite U, is increasing as U increases and approaches unity in the strong-coupling limit. This result supports the existence of the "antiferromagnetic" orbital order at half filling.

The "antiferromagnetic" orbital order is destroyed by doping the system away from half filling. This is illustrated in Fig. 4(b), where the staggered orbital order-parameter m is plotted as a function of filling n at different interactions $U=8t_\parallel$ (denoted by △) and $U=3t_\parallel$ (denoted by ∗). Figure 4(b) shows that the order-parameter m decreases sharply when n decreases, and disappears completely ($m=0$) at fillings $n \approx 0.85$ and $n \approx 0.94$ for $U=8t_\parallel$ and $U=3t_\parallel$, respectively. We
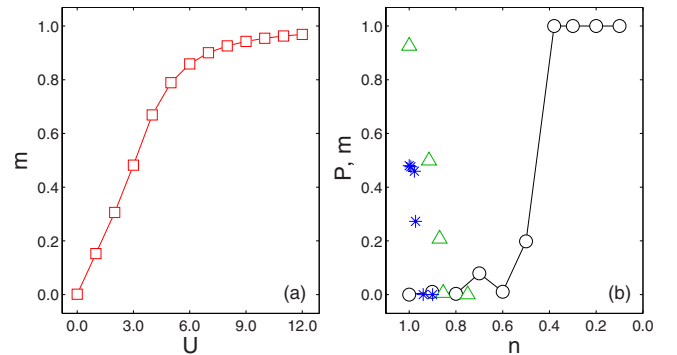

FIG. 4. (Color online) (a) Staggered orbital order-parameter m (□) as a function of interaction U at half filling. (b) Orbital polarization P at $U=8t_\parallel$ (○) and staggered orbital order-parameter m at $U=8t_\parallel$ (△), and $U=3t_\parallel$ (∗) as a function of filling n.

conclude that the "antiferromagnetic" orbital order at large U is more difficult to destroy than at small U. After $m=0$, the system enters a featureless "paramagnetic" orbital state.

C. Orbital order at low filling

As shown in the spectrum (see Figs. 2 and 3), the spinless p-band model has strong 1D character for each orbital due to the anisotropic hopping, and therefore its band structure has a Van Hove singularity[17] near the band edge. It is interesting to see whether or not this singularity can produce "ferromagnetic" orbital order at low filling [shown schematically in Fig. 1(c)].[41]

The question is subtle because the same Van Hove singularity present in the 1D single-band Hubbard model at low filling is not sufficient to obtain ferromagnetism. In particular, a Hartree-Fock argument provides the wrong conclusion that the ferromagnetic state should be lower in energy than the paramagnetic state at sufficiently low densities and large U in one dimension. This result is indeed contradicted by the rigorous Lieb-Mattis theorem,[42] which excludes ferromagnetism for the 1D Hubbard model as well as by an accurate analysis based on the Gutzwiller wave function.

While the Lieb-Mattis theorem does not apply to the present p-band model, we investigate here whether or not an instability of the totally polarized ferromagnetic state toward a variational, less polarized, and, ultimately, paramagnetic wave function can be found for the p-band model in the low-density and $U \rightarrow \infty$ limit. As trial wave functions for the less polarized state we use the Gutzwiller wave function, as well as a more general one, i.e., with lower energy. Despite this, we find that the totally polarized state, which, of course, can be solved exactly for an on-site interaction, always has the lowest energy. While we were not able so far to prove that the totally polarized state is the most stable one at sufficiently low filling, the fact that we have used a quite general trial wave function makes us confident that there should be no wave functions with a lower energy than the totally polarized state.

We consider a p-band model with N particles in a finite $L \times L$ square lattice with periodic boundary conditions (PBC). For simplicity, we take $t_\perp=0$ and $U=\infty$. Quite generally, we can expect that if the ferromagnetic phase has a lower energy with a finite gap to the paramagnetic state for these values of $t_\perp$ and U, its stability region should extend to some finite $t_\perp$ and U.

If $N \leq L$, it is quite clear that the lowest energy is obtained by putting all particles in the same orbital (say, p_x) on different "rows." In that case, each particle moves independently on its row, so that the kinetic energy is minimal and the interaction energy is zero. However, this cannot lead to the conclusion that the ferromagnetic state is stable at sufficiently low but finite density, since for $N \leq L$ the density vanishes in the thermodynamic limit. The crucial question is what happens for $N=L+1$; i.e., is it more convenient energetically to put the next particle in one of the already occupied rows in the p_x orbital, or to put it in a "column" in the p_y orbital? If the particle is added to the p_x orbital, the system is still in a full ferromagnetic state, and the energy change

ΔE_1 of this state with respect to the ground state with $N=L$, $|L\rangle_x$ (which has energy $E_0 = -2t_\parallel L$), is given by

$$\Delta E_1 = -2t_\parallel \cos\left(\frac{2\pi}{L}\right) \approx -2t_\parallel\left(1 - \frac{2\pi^2}{L^2}\right), \qquad (3)$$

where, in the last term, we have taken the large L limit. If we add the particle to the p_y orbital on one of the columns (no matter which one), the lowest-energy state cannot be determined exactly. Therefore, we approximate it by a trial wave function. The simplest one is the Gutzwiller wave function

$$|\psi\rangle = \prod_{\mathbf{r}} (1 - n_{\mathbf{r},x} n_{\mathbf{r},y}) d^\dagger_{(x=0,q_y=0),y}|L\rangle_x, \qquad (4)$$

where $d^\dagger_{(x,q_y),y}$ creates a particle on p_y orbitals on "column" (x) with y wave vector q_y. The energy increase can be easily evaluated as

$$\Delta E_2 = -2t_\parallel\left(1 - \frac{2}{L-1}\right). \qquad (5)$$

Clearly, this energy is larger than Eq. (3). The reason for this is that for the row where the p_y particle sits, the Gutzwiller wave function of the p_x particle has a sharp jump at the position of the p_y particle [see Eq. (4)]. This leads to an increase of $2t_\parallel/(L-1)$ in the kinetic energy of the p_x particle. A natural improvement consists in replacing the wave function of this row by a smooth sine function, $\sin(\pi x/L)$, which has much smaller energy increase. However, the overlap of this sin function with the wave function of the other rows, which is $\sqrt{1/L}$, is small, resulting in a large kinetic energy of the p_y particle. A proper choice is to linearly combine these two functions. This leads to the trial wave function

$$|\psi\rangle = \frac{1}{L}\sum_m c^\dagger_{(0,m),y}$$
$$\times \prod_n \sum_l \left[a_{m-n} + \sqrt{2}b_{m-n}\sin\left(\frac{\pi l}{L}\right)\right]c^\dagger_{(l,n),x}|0\rangle, \quad (6)$$

where (l,m) explicitly denotes the 2D coordinates of a position $\mathbf{r}$, and $l,m,n=0,1,\ldots,L-1$. Since we are using PBC, our assumption that the p_y particle is in the 0th column does not lead to a loss of generality. The coefficients a_{m-n} and b_{m-n} can be chosen, for simplicity, to be $a_{m-n}=\sin^2\frac{(n-m)\pi}{L}$, and $b_{m-n}=\cos^2\frac{(n-m)\pi}{L}$. This choice does not affect our conclusions, as discussed below. The energy increase for the state in Eq. (6) is given by

$$\Delta E_3 = -2t_\parallel\left(1 - \frac{\alpha}{L} + O(L^{-2})\right), \qquad (7)$$

where $\alpha \approx 0.5$ is a constant. A comparison of the energies of this trial wave function with the fully polarized ferromagnetic state, whose energy increase is $-2t_\parallel+O(L^{-2})$, shows that the latter has a lower energy. Notice that more general forms of the coefficients a_{m-n} and b_{m-n} do not change this conclusion, as they merely modify the coefficient α in Eq. (7), which, however, remains nonzero and positive.

The above results show that, although the spinless p-band model has strong 1D character, it is different from the 1D

Hubbard model. This can be seen by constructing a trial wave function in a similar way to Eq. (6) for the 1D Hubbard model with two particles.[43] In this case, the total energy for PBC is $-4t_\parallel+C/L^2+O(L^{-4})$ with $C=2\pi^2 t_\parallel$ for the paramagnetic state and $C=4\pi^2 t_\parallel$ for the ferromagnetic state,[43] i.e., the ferromagnetic state is unstable. This situation is quite different from the partly polarized state of the p-band model presented above with one particle in the p_y orbital and L particles in p_x orbital. In this case, the motion of the p_y particle is hindered by, and, at the same time, affects the motion of the other L particles in the p_x orbitals. This leads to a much larger energy increase than in the fully polarized ferromagnetic state.

After having discussed the stability of the ferromagnetic phase from a more accurate point of view, we return to the results of the VCA approximation in the low-filling region. In the ferromagnetic case it is necessary to introduce a different on-site energy between the two orbitals as a variational parameter. This is equivalent to using the cluster chemical potential and a "ferromagnetic" field. In the fully polarized case, the saddle point is given by the on-site energy of the empty orbital approaching infinity. To describe the ferromagnetic phase, we evaluate the orbital-polarization $P \equiv (n_x-n_y)/(n_x+n_y)$, where n_x and n_y are the average occupations of the p_x and p_y orbitals. Results for P as a function of filling for $U=8t_\parallel$ are plotted in Fig. 4(b) (denoted by ○). The orbital polarization P is calculated at the respective stationary point of Ω in each phase. As in Fig. 4(b), P vanishes at half filling and remains essentially zero down to a filling of $n\approx 0.6$. For $n<0.6$, P rapidly increases as n decreases, and rapidly saturates ($P=1$) at $n\approx 0.38$ indicating a full ferromagnetic orbital order state.

We should stress that one must be careful when interpreting the VCA results at low filling. First, we cannot exclude that finite-size effects, originating from the limited size of the reference cluster, could affect the ordered state found in our calculation. This could be the case when the exact self-energy is long ranged, so that it cannot be accurately described by the self-energy of a small reference system. Second, the density obtained by VCA shows small discontinuities when the reference cluster changes its particle number.[44] Therefore, it is difficult for VCA to determine the exact critical point for the onset of ferromagnetic orbital ordering as a function of filling.

Summarizing this section, our combined VCA and variational results are a strong indication, although not a proof, for the presence of an orbital ferromagnetic state at low-density and sufficiently large U in the p-band model. An exact proof for the absence or existence of ferromagnetism at low densities in the p-band model (similar to the Hubbard model)[41] would be welcome. However, it is beyond the goal of the present paper.

D. Momentum distribution

In this section, we present results for the momentum distribution, as this quantity is directly accessible experimentally,[20] and can be used to detect the possible occurrence of orbital ordering. Our results are shown in Fig. 5.
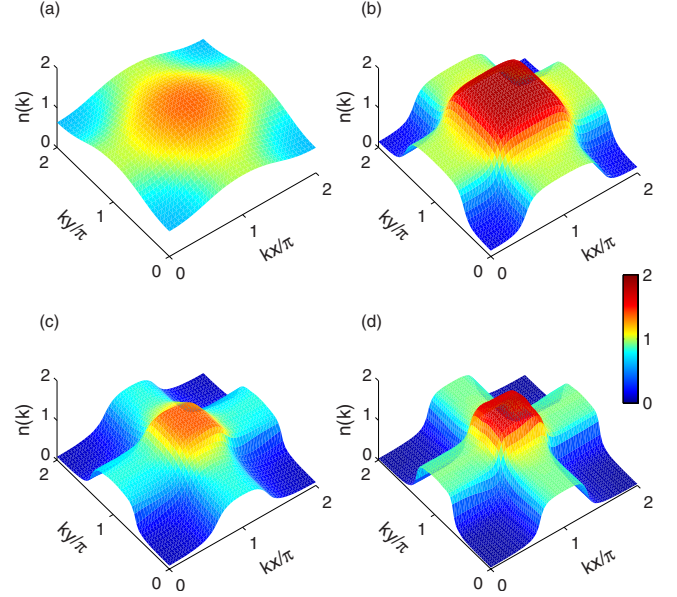

FIG. 5. (Color online) Momentum distribution $n(k)$ for different values of the interaction U and of the filling n, with $t_\perp=-0.05t_\parallel$. (a) $U=10t_\parallel$ and $n=1.0$; (b) $U=3t_\parallel$ and $n=1.0$; (c) $U=10t_\parallel$ and $n=0.6$; (d) $U=3t_\parallel$ and $n=0.6$.

For half filling and small values of the interaction U [Fig. 5(b)], the momentum distribution can approximately be seen as the superposition of two 1D noninteracting gases traveling in the two directions x and y. Double occupations are present in k space in the middle square region of the Brillouin zone. While double occupation is allowed for small U, it is strongly suppressed for strong interactions. Therefore, for large U, the momentum distribution is flattened and covers the whole BZ [see Fig. 5(a)]. By decreasing the filling away from half filling the suppression of double occupation weakens, as can be seen in Figs. 5(c) and 5(d) for $n=0.6$. The reason is that the system has a strongly dispersive spectrum [see Fig. 2(c)] and, therefore, it is no longer in a Mott state. The fact that particles can move quite free in the lattice gives rise to the possibility of double occupation even at large interactions.

Finally, we briefly discuss the experimental signatures. The momentum distribution of fermions in the excited p-band (see Fig. 5) is different from that of fermions in the lowest s-band,[20] e.g., in the weak interacting regime. This can be directly observed in the time-of-flight (TOF) images. The antiferromagnetic orbital order can be detected by analyzing the noise correlation function from TOF images. In the noise correlation spectrum, the s-band fermions produce the antibunching dips at the usual reciprocal wave vector of square lattice.[45,46] However, the p-band fermions in the antiferromagnetic orbital order state contribute new dips at the reciprocal wave vector of doubled unit cell.[21]

IV. CONCLUSION

In summary, we have studied a model for spinless p-band fermions in optical lattices using the variational cluster approach, and, partly, a variational wave function. We have

computed its single-particle spectral function in a wide range of fillings and found a strongly dispersive spectrum at incommensurate fillings. By calculating the staggered orbital order parameter, we showed that the system is in a staggered ("antiferromagnetic") orbital state at half filling, which is destroyed by doping and evolves into a paramagnetic state. In the low-density limit and for $U = \infty$, we studied the stability of a fully polarized ferromagnetic state by constructing a trial wave function, which extends the Gutzwiller trial state. In contrast to the one- and two-dimensional Hubbard model we did not find an instability of the ferromagnetic state toward the paramagnetic solution. In particular, for the trial wave function of Eq. (6) (which is more general than the Gutzwiller wave function), the ferromagnetic state is lower in energy than the paramagnetic one. Finally, we have computed, by VCA, the momentum distribution and studied its evolution as a function of interaction and filling.

ACKNOWLEDGMENTS

APPENDIX: FREQUENCY INTEGRATION

The sum over Matsubara frequencies in Eq. (2) can be carried out either (i) directly (see also Ref. 47) or (ii) by the usual procedure[48] of distorting the contour to the real axis. For a numerical sum, and especially for the corresponding integral at $T=0$, both procedures present their advantages and disadvantages. In case (i) one should first extract the asymptotic (for large $i\omega_n$) part of the integrand and carry out the corresponding sum/integral analytically. In case (ii) there is no such problem, as the contribution to the integral at an infinitesimal distance $\delta \to 0$ from the real axis is nonzero only within the region where the spectral function is nonzero. However, due to the pole structure of the integrand, one has to take a finite δ for numerical purposes. This reduces the precision and introduces additional complications coming from the fact that at large ω the integrand goes like $1/\omega^2$.

The best solution is to distort the integral to the contour indicated in Fig. 6. For a sum over Matsubara frequencies $\omega_n = 2\pi T(n + \frac{1}{2})$ of a function $g(z)$ of the complex variable z, which is analytic everywhere except on the real axis, we have

$$T \sum_{n=-\infty}^{+\infty} e^{i\omega_n 0^+} g(i\omega_n) = -\frac{1}{2\pi i} \oint_C e^{z0^+} f_F(z) g(z) dz. \quad \text{(A1)}$$

Here, C is the usual contour of the complex plane encircling the Matsubara frequencies $i\omega_n$, $f_F(z) = (\exp\frac{z}{T} + 1)^{-1}$ is the Fermi function, and 0+ is a positive infinitesimal. With the usual conditions that $g(z) \to 0$ for $|z| \to \infty$, and that

$$g(z^*) = g(z)^*, \quad \text{(A2)}$$

we can further distort the contour C to the contour indicated in Fig. 6. Here, C_1 and C_1' are semicircles at infinity, so that
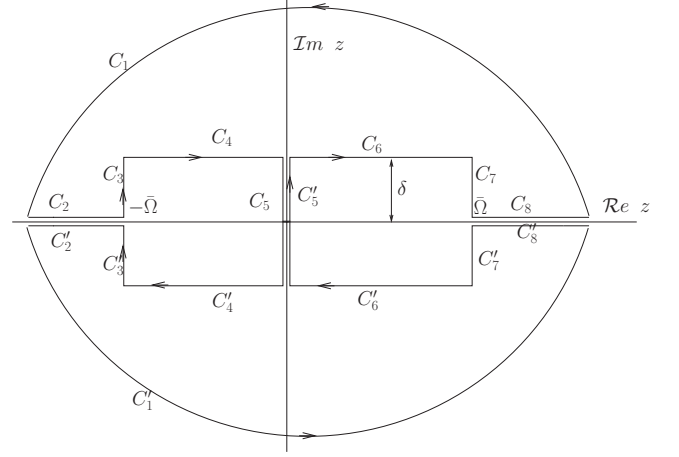

FIG. 6. Contour in the complex plane in which the frequency integration is carried out.

their contribution vanish, C_2 and C_8, and C_2' and C_8' are infinitesimally close to the real axis, as in the usual procedure. C_5 and C_5' are infinitesimally close to the imaginary axis, while C_4 and C_6, and C_4' and C_6' can have an arbitrary finite-distance δ from the real axis. We take $\bar{\Omega}$ as some upper limit of the spectrum; i.e.,

$$\text{Im } g(\omega + i0^+) = 0 \quad \text{for any} \quad |\omega| > \bar{\Omega}. \quad \text{(A3)}$$

By calling

$$F(z) \equiv g(z) f_F(z) \quad \text{(A4)}$$

we can first write the contributions to Eq. (A1) from the "horizontal" paths

$$S_h = -\frac{1}{\pi} \int_{C_2 + C_4 + C_6 + C_8} \text{Im } F(z) dz. \quad \text{(A5)}$$

Notice that for $\delta \to 0$ one recovers the usual expression,[48] and there is obviously no contribution from the "vertical" paths. The contributions from C_2 and C_8 vanish, due to Eq. (A3) $[f_F(z)$ is analytic across the real axis]. Therefore, we are left with

$$S_h = -\frac{1}{\pi} \int_{-\bar{\Omega}}^{\bar{\Omega}} \text{Im}[g(\omega + i\delta) f_F(\omega + i\delta)] d\omega. \quad \text{(A6)}$$

The advantage of taking a finite δ is that the integrand is smooth and one only needs few ω points in the numerical integration in order to achieve a good accuracy, in contrast to the conventional case of small δ. For $T=0$ Eq. (A6) reduces to

$$S_h = -\frac{1}{\pi} \int_{-\bar{\Omega}}^{0} \text{Im } g(\omega + i\delta) d\omega. \quad \text{(A7)}$$

The rest of the integral is given by the "vertical" paths, for example, the contribution from C_3 and C_3' is given by

$$-\frac{1}{2\pi i}\int_{C_3+C_3'}\cdots = \frac{i}{2\pi}\left[\int_0^\delta F(-\bar\Omega+ix)idx\right.$$
$$\left.-\int_0^\delta F(-\bar\Omega-ix)(-i)dx\right]$$
$$=-\frac{1}{\pi}\int_0^\delta \text{Re}\,F(-\bar\Omega+ix)dx \qquad \text{(A8)}$$

and similarly for the contribution from C_7 and C_7',

$$-\frac{1}{2\pi i}\int_{C_7+C_7'}\cdots = \frac{1}{\pi}\int_0^\delta \text{Re}\,F(\bar\Omega+ix)dx. \qquad \text{(A9)}$$

The latter contribution vanishes for $T=0$ or can be made exponentially small by taking $\bar\Omega/T\gg1$. The contribution from the "central" vertical paths C_5 and C_5' is simply given by the original sum over Matsubara frequencies, however only for $|\omega_n|<\delta$ (we must be wise and choose δ not to co-

incide with a Matsubara frequency for $T>0$). Denoting by $\omega_{n_{\max}}$ the corresponding maximum frequency, we have

$$-\frac{1}{2\pi i}\int_{C_5+C_5'}\cdots = 2T\sum_{n=0}^{n_{\max}}\text{Re}\,g(i\omega_n), \qquad \text{(A10)}$$

which for $T=0$ becomes

$$\frac{1}{\pi}\int_0^\delta \text{Re}\,g(ix)dx. \qquad \text{(A11)}$$

The contributions, Eqs. (A8)–(A10), are the additional integrals to be carried out to compensate for the nonvanishing value of δ. We stress that the result is exact for any (even large) value of $\delta>0$. The numerical advantage is that the integrand is smooth everywhere except for small temperatures and on the path C_5 near $\omega_n=0$ whenever $g(\omega)$ has poles close to $\omega=0$. Moreover, all integrals are carried out in a finite domain, so there is no need to carry out extrapolations.

[1] I. Bloch, J. Dalibard, and W. Zwerger, Rev. Mod. Phys. **80**, 885 (2008).

[2] M. Greiner, O. Mandel, T. Esslinger, T. W. Hänsch, and I. Bloch, Nature (London) **415**, 39 (2002).

[3] D. Jaksch, C. Bruder, J. I. Cirac, C. W. Gardiner, and P. Zoller, Phys. Rev. Lett. **81**, 3108 (1998).

[4] T. Müller, S. Fölling, A. Widera, and I. Bloch, Phys. Rev. Lett. **99**, 200405 (2007).

[5] A. Isacsson and S. M. Girvin, Phys. Rev. A **72**, 053604 (2005).

[6] W. V. Liu and C. Wu, Phys. Rev. A **74**, 013607 (2006).

[7] M. Imada, A. Fujimori, and Y. Tokura, Rev. Mod. Phys. **70**, 1039 (1998).

[8] Y. Kamihara, T. Watanabe, M. Hirano, and H. Hosono, J. Am. Chem. Soc. **130**, 3296 (2008).

[9] E. Dagotto, T. Hotta, and A. Moreo, Phys. Rep. **344**, 1 (2001).

[10] R. A. de Groot, F. M. Mueller, P. G. van Engen, and K. H. J. Buschow, Phys. Rev. Lett. **50**, 2024 (1983).

[11] L. Chioncel, E. Arrigoni, M. I. Katsnelson, and A. I. Lichtenstein, Phys. Rev. Lett. **96**, 137203 (2006).

[12] C. Wu, W. V. Liu, J. Moore, and S. Das Sarma, Phys. Rev. Lett. **97**, 190406 (2006).

[13] A. B. Kuklov, Phys. Rev. Lett. **97**, 110405 (2006).

[14] C. Wu, D. Bergman, L. Balents, and S. Das Sarma, Phys. Rev. Lett. **99**, 070401 (2007).

[15] C. Xu and M. P. A. Fisher, Phys. Rev. B **75**, 104428 (2007).

[16] K. Wu and H. Zhai, Phys. Rev. B **77**, 174431 (2008).

[17] L. Wang, X. Dai, S. Chen, and X. C. Xie, Phys. Rev. A **78**, 023603 (2008).

[18] S. Zhang, H. Hung, and C. Wu, arXiv:0805.3031 (unpublished).

[19] A. Browaeys, H. Häffner, C. McKenzie, S. L. Rolston, K. Helmerson, and W. D. Phillips, Phys. Rev. A **72**, 053605 (2005).

[20] M. Köhl, H. Moritz, T. Stöferle, K. Günter, and T. Esslinger, Phys. Rev. Lett. **94**, 080403 (2005).

[21] E. Zhao and W. V. Liu, Phys. Rev. Lett. **100**, 160403 (2008).

[22] C. Wu, Phys. Rev. Lett. **100**, 200406 (2008).

[23] M. Daghofer, K. Wohlfeld, A. M. Oleś, E. Arrigoni, and P.

Horsch, Phys. Rev. Lett. **100**, 066403 (2008).

[24] C. Wu and S. Das Sarma, Phys. Rev. B **77**, 235107 (2008).

[25] M. Potthoff, M. Aichhorn, and C. Dahnken, Phys. Rev. Lett. **91**, 206402 (2003).

[26] C. Dahnken, M. Aichhorn, W. Hanke, E. Arrigoni, and M. Potthoff, Phys. Rev. B **70**, 245110 (2004).

[27] C. Gros and R. Valenti, Phys. Rev. B **48**, 418 (1993).

[28] D. Sénéchal, D. Perez, and M. Pioro-Ladrière, Phys. Rev. Lett. **84**, 522 (2000).

[29] S. G. Ovchinnikov and I. S. Sandalov, Physica C **161**, 607 (1989).

[30] M. Potthoff, Eur. Phys. J. B **32**, 429 (2003).

[31] M. Potthoff, Eur. Phys. J. B **36**, 335 (2003).

[32] M. Aichhorn and E. Arrigoni, Europhys. Lett. **72**, 117 (2005).

[33] M. Aichhorn, E. Arrigoni, M. Potthoff, and W. Hanke, Phys. Rev. B **74**, 024508 (2006).

[34] R. Freund, in *Templates for the Solution of Algebraic Eigenvalue Problems: A Practical Guide*, edited by Z. Bai, J. Demmel, J. Dongarra, A. Ruhe, and H. van der Vorst (SIAM, Philadelphia, 2000), Chap. 4.6.

[35] M. Aichhorn, E. Arrigoni, M. Potthoff, and W. Hanke, Phys. Rev. B **74**, 235117 (2006).

[36] M. G. Zacher, R. Eder, E. Arrigoni, and W. Hanke, Phys. Rev. B **65**, 045109 (2002).

[37] D. Sénéchal, P.-L. Lavertu, M.-A. Marois, and A.-M. S. Tremblay, Phys. Rev. Lett. **94**, 156404 (2005).

[38] S. Brehm, E. Arrigoni, M. Aichhorn, and W. Hanke, arXiv:0811.0552 (unpublished).

[39] G. Martinez and P. Horsch, Phys. Rev. B **44**, 317 (1991).

[40] H. Eskes, M. B. J. Meinders, and G. A. Sawatzky, Phys. Rev. Lett. **67**, 1035 (1991).

[41] P. Fazekas, *Lecture Notes on Electron Correlation and Magnetism* (World Scientific, Singapore, 1999).

[42] H. Tasaki, Prog. Theor. Phys. **99**, 489 (1998).

[43] F. Gebhard, *The Mott Metal-Insulator Transition—Models and Methods*, Springer Tracts in Modern Physics Vol. 137 (Springer,

Heidelberg, 1997).

[44] M. Balzer, W. Hanke, and M. Potthoff, Phys. Rev. B **77**, 045133 (2008).

[45] E. Altman, E. Demler, and M. D. Lukin, Phys. Rev. A **70**, 013603 (2004).

[46] T. Rom, T. Best, D. van Oosten, U. Schneider, S. Fölling, B. Paredes, and I. Bloch, Nature (London) **444**, 733 (2006).

[47] D. Sénéchal, arXiv:0806.2690 (unpublished).

[48] A. L. Fetter and J. D. Walecka, *Quantum Theory of Many-Particle Systems* (McGraw-Hill, New York, 1971).